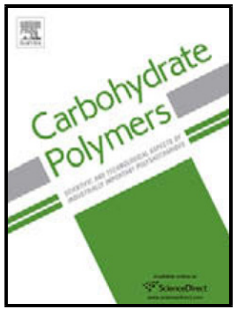

Title: Starch/microcrystalline cellulose hybrid gels as gastric-floating drug delivery systems

Authors: Jinchuan Xu, Xiaoyan Tan, Ling Chen, Xiaoxi Li, Fengwei Xie

PII: S0144-8617(19)30350-9
DOI: https://doi.org/10.1016/j.carbpol.2019.03.078
Reference: CARP 14747

To appear in:

Received date: 15 February 2019
Revised date: 23 March 2019
Accepted date: 23 March 2019

Please cite this article as: Xu J, Tan X, Chen L, Li X, Xie F, Starch/microcrystalline cellulose hybrid gels as gastric-floating drug delivery systems, *Carbohydrate Polymers* (2019), https://doi.org/10.1016/j.carbpol.2019.03.078

Starch/microcrystalline cellulose hybrid gels as gastric-floating drug delivery systems

Jinchuan Xu [a], Xiaoyan Tan [a,b], Ling Chen [a,*] , Xiaoxi Li [a], Fengwei Xie [c,d,*]

[a] *Ministry of Education Engineering Research Center of Starch & Protein Processing, Guangdong Province Key Laboratory for Green Processing of Natural Products and Product Safety, School of Food Science and Engineering, South China University of Technology, Guangzhou, Guangdong, 510640, China*

[b] *College of Food Science and Light Industry, Nanjing Tech University, Nanjing, Jiangsu 211816, China*

[c] *International Institute for Nanocomposites Manufacturing (IINM), WMG, University of Warwick, Coventry CV4 7AL, United Kingdom*

[d] *School of Chemical Engineering, The University of Queensland, Brisbane, Qld 4072, Australia*

[*]Corresponding author. E-mail address: felchen@scut.edu.cn (L. Chen)

[*]Corresponding author. E-mail address: D.Xie.2@warwick.ac.uk, f.xie@uq.edu.au (F. Xie).

Graphical Abstract

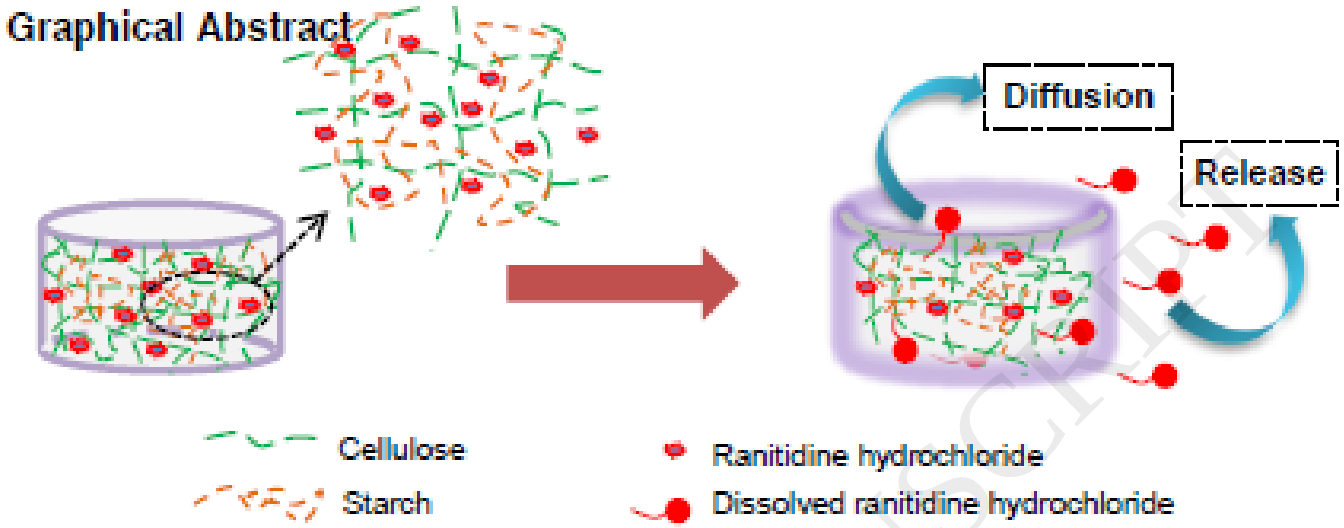

Highlights:

- ✓ A starch/cellulose-based gastric-floating drug delivery system was established
- ✓ Polysaccharide gels had a porous, three-dimensional network structure
- ✓ The gels had low-density and presented suitable texture and swellability
- ✓ The gels exhibited excellent floatability and sustained drug release behaviour
- ✓ The release was both diffusion-controlled and osmotic pressure-driven

Abstract: We report hybrid gels based on a high-amylose starch and microcrystalline cellulose with demonstrated properties for gastric-floating drug delivery purposes. The starch/cellulose gels were prepared by ionic liquid dissolution and regeneration, resulting in a continuous surface and a porous interior and a type-II crystalline structure of cellulose. These polysaccharide gels displayed

satisfactory elasticity (0.88), recovery (0.26–0.36) and equilibrium swelling (1013–1369%). The hybrid gels were loaded with ranitidine hydrochloride as a model drug and subsequently, low-density starch/cellulose tablets were fabricated by vacuum-freeze-drying. *In vitro* tests in a simulated gastric fluid indicate that the 3:7 (wt./wt.) starch/cellulose system could maintain the buoyancy for up to 24 h with a release of 45.87% for the first 1 h and a sustained release for up to 10 h. Therefore, our results have demonstrated the excellent gastric-floating ability and sustainable drug release behavior of the starch/cellulose hybrid gels.

Keywords: Gastric-floating drug delivery system; Starch/microcrystalline cellulose hybrid materials; Ionic liquids; Gels; Natural polymers; Polysaccharides

1 Introduction

In recent years, natural polymers such as cellulose and starch have attracted considerable attention for developing environmentally friendly and biocompatible materials. These two polysaccharides are two of the most abundant carbohydrates in the plant world and are composed of the same unit structure, namely, the glucose unit, but linked through the different β-1,4- and α-1,4-glycosidic bonds, respectively (Kadokawa, Murakami, Takegawa, & Kaneko, 2009). Cellulose and starch have completely different roles in nature, with the former being a structural material and the latter functioning for energy storage (Kadokawa et al., 2009). Cellulose is a polydispersed linear homopolymer composed of D-glucopyranose units linked with β-1,4-glycosidic bond, including free hydroxyl groups (─OH) at the C-2, C-3, and C-6 atoms (Vilarinho, Sanches Silva, Vaz, & Farinha, 2018). Microcrystalline cellulose (MCC) has a smaller degree of polymerization, where the amorphous regions have been removed by acid hydrolysis and it has the advantage of a high specific surface area compared to other conventional cellulose fibers (Mathew, Oksman, & Sain, 2005). Starch occurs naturally as semicrystalline granules, made up of two polymer components, namely amylose, which is essentially linear, and amylopectin, which is highly branched (Wang & Copeland, 2013). High-amylose starches, which have been obtained by genetic modification, present varied properties such as a higher gelatinization temperature (Yang et al., 2016).

Cellulose is the most abundant biopolymer in nature and has several traditional applications such as packaging, clothing, and biomedical materials (Klemm, Heublein, Fink, & Bohn, 2005). The physical and chemical properties of cellulose are mainly determined by the intra-/intermolecular hydrogen-bonding interactions. The inherent, strong hydrogen bonds make cellulose highly resistant

to processing. As a result, considerable efforts have been devoted to improving the processability of cellulose (Vilarinho et al., 2018). On the other hand, starch is also an abundant carbohydrate source of plant species and has several advantages such as low-cost, biodegradability, and nontoxicity (Gross & Kalra, 2002). Therefore, starch can be used for applications where biocompatibility and safety are required, such as edible and drug carrier materials. However, inherent, strong hydrogen bonds also predominantly exist between starch chains, resulting in poor solubility in most common organic solvents, causing difficulties in the processing and in extending the functionality of starch. Therefore, it is important to find appropriate solvents for effectively dissolving starch and cellulose to improve the functionality of these two polysaccharides. For blending cellulose and starch, considerable efforts have been devoted to exploring new solvent systems such as dimethyl sulfoxide (DMSO) (Zhong, Yokoyama, Wang, & Shoemaker, 2006), concentrated inorganic alkali solutions (e.g., KOH and NaOH) (Builders, Bonaventure, Tiwalade, Okpako, & Attama, 2010; Wang, Chang, & Zhang, 2010), zinc chloride aqueous solution (Shang, Jiang, Wang, Liu, & Xie, 2019), *N*-methylmorpholine-*N*-oxide (NMMO) (Koganti, Mitchell, MacNaughtan, Hill, & Foster, 2015; Wendler et al., 2011), and ionic liquids (Liu & Budtova, 2012; Wu, Wang, Li, Li, & Wang, 2009). However, these solvents also have their drawbacks associated with, for example, separation difficulties, environmental pollutions, and undesirable material properties.

Ionic liquids (ILs) are commonly defined as salts that have melting temperatures below 100 °C, which could form liquids that are comprised entirely of cation and anions (Forsyth, Pringle, & MacFarlane, 2004). ILs have been claimed as “green solvents” for natural polymers such as cellulose and starch (Chen, Xie, Li, & Chen, 2018; Stevenson, Biswas, Jane, & Inglett, 2007). In particular,

great attention has been paid to imidazolium-based ILs such as 1-butyl-3-methylimidazolium chloride ([Bmim]Cl) (Li, Zhang, & Tian, 2016; Zarski, Ptak, Siemion, & Kapusniak, 2016), 1-allyl-3-methylimidazolium chloride ([Amim]Cl) (Xia et al., 2016), and 1-ethyl-3-methylimidazolium acetate ([Emim][OAc]) (Froschauer et al., 2013; Pang et al., 2015).

Gastroretentive drug delivery systems (GRDSs) were designed to prolong the release and enhance the absorption of drugs in the stomach or the upper gastrointestinal tract. To achieve gastric retention and sustained drug release, many approaches have been developed including gastric floating drug delivery systems (GFDDSs), swelling and expanding systems, mucoadhesive or bioadhesive systems, high-density systems, ultraporous hydrogel systems, and magnetic systems (Fassihi, 2004; Kansal, Garg, Awasthi, Singodia, & Kulkarni, 2011). Compared with the other systems, GFDDSs can float over the gastric contents due to their lower bulk density than those of the gastric contents. Furthermore, unlike the mucoadhesive systems and swelling systems, GFDDSs present no risk of gastric injuries and minimal side effects (Arora, Ali, Ahuja, Khar, & Baboota, 2005; Kansal et al., 2011).

Thus, the focus of this work was to develop gastric-floating sustained-release tablets with a low density based on starch and cellulose. Different formulations of hybrid gels based on a high-amylose starch and MCC were prepared by dissolving the polysaccharides in [Emim][OAc]. The structures and properties of the resulting hybrid gels were thoroughly investigated, and the related gastric-floating drug delivery systems were constructed. The results from this study are expected to provide relevant information for the rational design of new polysaccharide-derived gel materials with suitable drug loading and releasing behaviors.

2 Materials and methods

2.1 Materials

The starch used in this study was Gelose 50 (G50), which has an amylose/amylopectin ratio of 50/50 and was supplied by Ingredion ANZ Pty Ltd. (Lane Cove, NSW 2066, Australia). Microcrystalline cellulose (MCC) PH101, of food grade, was purchased from Linghu Xinwang Chemical Co., Ltd. (Huzhou, China). 1-Ethyl-3-methylimidazolium acetate ionic liquids ([Emim][OAc] ILs, ≥95% purity, *ca.* 1200 ppm water content) was produced by IoLiTec Ionic Liquids Technologies GmbH (Salzstraße184, D-74076 Heilbronn, Germany). Ranitidine hydrochloride (Pharmaceutical grade, >99% purity) was produced by Wuhan Hezhong Biochemical Manufacturing Co., Ltd (Hubei, China). Ranitidine hydrochloride capsules (Pharmaceutical grade, 0.15 g per capsule) was purchased from Shanghai Huangxiang Tieli Lantian Pharmaceutical Co., Ltd. (Shanghai China). Before use, G50 and MCC were dried at 70 °C in a vacuum oven (DZF-6020, Shanghai Yiheng Scientific Instrument Co., Ltd., China) for 24 h; and [Emim][OAc] was kept in a vacuum oven at 90 °C for 24 h.

2.2 Preparation of G50/MCC hybrid gels

The preparation of G50/MCC gels followed our previous studies (Liu, Tan, Li, Chen, & Xie, 2018; Tan, Li, Chen, & Xie, 2016; Tan, Chen, Li, & Xie, 2019). The polysaccharides with a total concentration of 9 wt.% in [Emim][OAc] but varied G50/MCC ratios (10:0, 7:3, 5:5, 3:7, and 0:10, wt./wt.). The dissolution process was carried out in a sealed, jacketed glass vessel with magnetic stirring at 90 °C for 2.5 h to ensure complete dissolution. Regenerated G50/MCC hybrids were

obtained via a dissolution-coagulation route. Deionized water was used as an anti-solvent for precipitating the G50/MCC hybrids from [Emim][OAc]. The solutions were poured into deionized water to obtain coagulated G50/MCC gels, which were washed with more deionized water at room temperature. The samples were freeze-dried under vacuum using a freeze-dryer (FDU-1200, EYELA, Japan). For the following discussion, samples are coded such as G50-H, 7/3 G50/MCC-H, 5/5 G50/MCC-H, 3/7 G50/MCC-H, and MCC-H were used, where, typically, "7/3 G50/MCC-H" means the G50/MCC ratio is 7:3 in weight and "H" indicates the prepared gel.

2.3 Scanning electron microscopy (SEM)

The morphologies of G50/MCC hybrid materials were studied using an EVO18 scanning electron microscope (Zeiss, Germany). Before microscopic observation, the samples were sprinkled on a double-sided adhesive tape mounted on an aluminum specimen stub and coated for 2 min with a thin layer of gold using a 108-auto sputter coater (Cressington Scientific Instruments Ltd., UK). The accelerating voltage of the SEM was 10 kV.

2.4 Small-angle X-ray scattering (SAXS)

A SAXSess SAXS system (Anton Paar, Austria), operated at 50 mA and 40 kV, using Cu Ka radiation with a wavelength of 0.1542 nm as the X-ray source was applied to perform SAXS measurements. The prepared G50/MCC gels after coagulation were taken out from the water with the removal of excess water using filter paper and were cut into 2 × 0.2 cm rectangles. Then, each sample was placed in a paste sample cell and was exposed to the incident X-ray monochromatic

beam for 10 min. All data were normalized and the background and smeared intensities were removed using the SAXSquant 3.0 software.

2.5 X-ray Diffraction (XRD)

X-ray diffraction (XRD) analysis was conducted on an X'Pert PRO X-ray diffractometer (PANalytical, Netherlands) with Cu-Kα radiation at a wavelength of 0.1542 nm, operated at 40 mA and 40 kV. The scanning was performed with a diffraction angle (2θ) range from 4° to 50°, a scanning speed of 10°/min, and a step size of 0.033°. All measurements were undertaken in triplicate.

Using MDI Jade 6.0 software, the crystallinity (X_c) could be computed based on XRD curves between 5° and 30° by Eq.(1):

$$X_c(\%) = \frac{A_c}{A_c + A_a} \times 100\% \qquad (1)$$

where A_c and A_a are the integrated areas of all crystalline peaks and the amorphous halo on the X-ray diffractogram, respectively. In the software, cubic spline was selected for point sampling and the sampling threshold (in Poisson sigmas of counting statistics) was set to be 4.

2.6 Attenuated total reflectance Fourier-transform infrared (ATR-FTIR) spectroscopy

ATR-FTIR spectra were collected on a Nicolet 5700 FTIR spectrometer (Thermo Electron Corp, Madison, WI, USA) equipped with a Nicolet Smart Orbit ATR accessory incorporating a diamond internal reflection element. For each spectrum, 64 scans were taken in the wavenumber range of 4000–400 cm^{-1} at a resolution of 4 cm^{-1}. Each spectrum was recorded against air as the background. Three replicated measurements were recorded for each sample.

2.7 Texture profile analysis (TPA)

Texture profiles were analyzed by a TAXT texture analyzer (Stable Microsystems, Surrey, UK) equipped with a cylindrical P6 (6 mm diameter) stainless steel compression probe. The gel samples (15 mm in diameter and 6 mm in height) were compressed to 30% of their original heights. The probe speed was set to be 0.5 mm/s for the test. All measurements were repeated for 6 times. The TPA parameters including hardness, elasticity, cohesiveness, gumminess, and recovery were computed using the Texture Expert software supplied with the instrument.

2.8 Equilibrium swelling ability

The classical gravimetric method was used to measure the equilibrium swelling ratios (*ESR*s) of the gels. Swelling studies were performed in distilled water at 37 °C. The gel samples were immersed and swollen in distilled water for 3 days to reach the equilibrium states. Then, excess water on the swollen gel surface was removed by filter paper and the gels were weighed. Taking the average value of three measurements for each sample, and *ESR* is calculated according to Eq. (2):

$$ESR(\%) = \frac{W_s - W_d}{W_d} \times 100\% \qquad (2)$$

In this equation, W_s is the weight of the gel sample in the swollen equilibrium and W_d is the weight of the dried gel.

2.9 Preparation of simulated gastric fluid (SGF)

A simulated gastric fluid of pH 1.2 was prepared by adding 7 mL of concentrated HCl (37%) into 500 mL distilled water, which was added with 2 g of NaCl and more distilled water to make the volume to be 1 L (Moursy, Afifi, Ghorab, & El-Saharty, 2003).

2.10 Floatability

Desired floating in gastric fluids is the key to a successful gastric-floating drug delivery system. For ideal gastric floating, the system should float for 5 min and can then maintain the floating state for 8 h in a simulated gastric fluid (SGF). The *in vitro* floating performance of G50/MCC tablets was studied in the SGF (37 °C, 200 mL, pH=1.2) and the floatation time and continuous floating time were recorded by direct observation.

2.11 In vitro drug load and release tests

A mold (17 mm×20 mm) was used to prepare G50/MCC tablets. The tablets were loaded in a ranitidine hydrochloride aqueous solution at 4 °C in the dark for 48 h. Then, the tablets were rinsed twice with distilled water and freeze-dried under vacuum. The tablets after drug loading were coded as G50-T, 7/3 G50/MCC-T, 5/5 G50/MCC-T, 3/7 G50/MCC-T, MCC-T, where "T" indicates tablets. The drug loading percentage is defined according to Eq. (3):

$$\text{Drug loading percentage (\%)} = \frac{C_0V_0 - C_1V_1}{m} \times 100\% \quad (3)$$

In this equation, C_0 and V_0 are the concentration and volume of ranitidine hydrochloride, respectively, before drug loading; C_1 and V_1 are the concentration and volume of ranitidine hydrochloride, respectively, after drug loading; and m is the mass of the dry matter of G50/MCC gels.

The drug release test was undertaken according to the drug release determination Method I of the Pharmacopoeia of the People's Republic of China. The commercial ranitidine hydrochloride capsules were used for comparison. The testing medium was 200 mL of the SGF. The conditions

used were basket rotation speed of 100 r/min and temperature of 37±0.5 °C. At specified times (15, 30, 60, 90, 120, 180, 240, 360, 480, and 600 min), a 1-mL aliquot was withdrawn to be mixed with the fresh SGF to make a 10-mL solution and the testing medium was filled with 1 mL of the fresh SGF. The collected samples were shaken and passed through a 0.22 μm filter membrane, before their UV absorbances at 313 nm were measured. The accumulated drug release percentage (Q) is defined according to Eq. (4):

$$Q\ (\%) = \frac{\sum_{i=1}^{n-1} C_i V_i + C_n V}{W} \times 100\% \qquad (4)$$

In this equation, C_i or C_n (g/mL) is the concentrations of ranitidine hydrochloride at a certain time (i or n) in the testing medium; V_i (1 mL) is the volume of the collected aliquot (1 mL) of the testing medium; V is the total volume of the testing medium; and W (g) is the total mass of ranitidine hydrochloride in the G50/MCC tablets.

2.12 Statistical analysis

The results were reported as the mean values and standard deviations and were analyzed using the least significant difference test (LSD-test). Significance analysis was carried out using Duncan's multiple-range test. All data analyses were performed using the SPSS (Version 23.0) software. The significance level was set at $p < 0.05$.

3 Results and discussion

3.1 Morphology

Fig. 1 shows the SEM images of the surfaces of G50/MCC gels with different ratios. It can be observed that all G50/MCC gels had a cohesive surface without cracks. No phase separation between

G50 and MCC could be observed, indicating good compatibility between the two polysaccharides. For regeneration, the surface of G50/MCC hybrid materials was first exposed to water for removing [Emim][OAc]. This would result in an immediate establishment of hydrogen bonding in the surface resulting in a dense surface structure after vacuum-freeze-drying. Here, G50-H is not shown as it was not well-formed during regeneration due to its unstable network structure, which is not conducive to SEM observation.

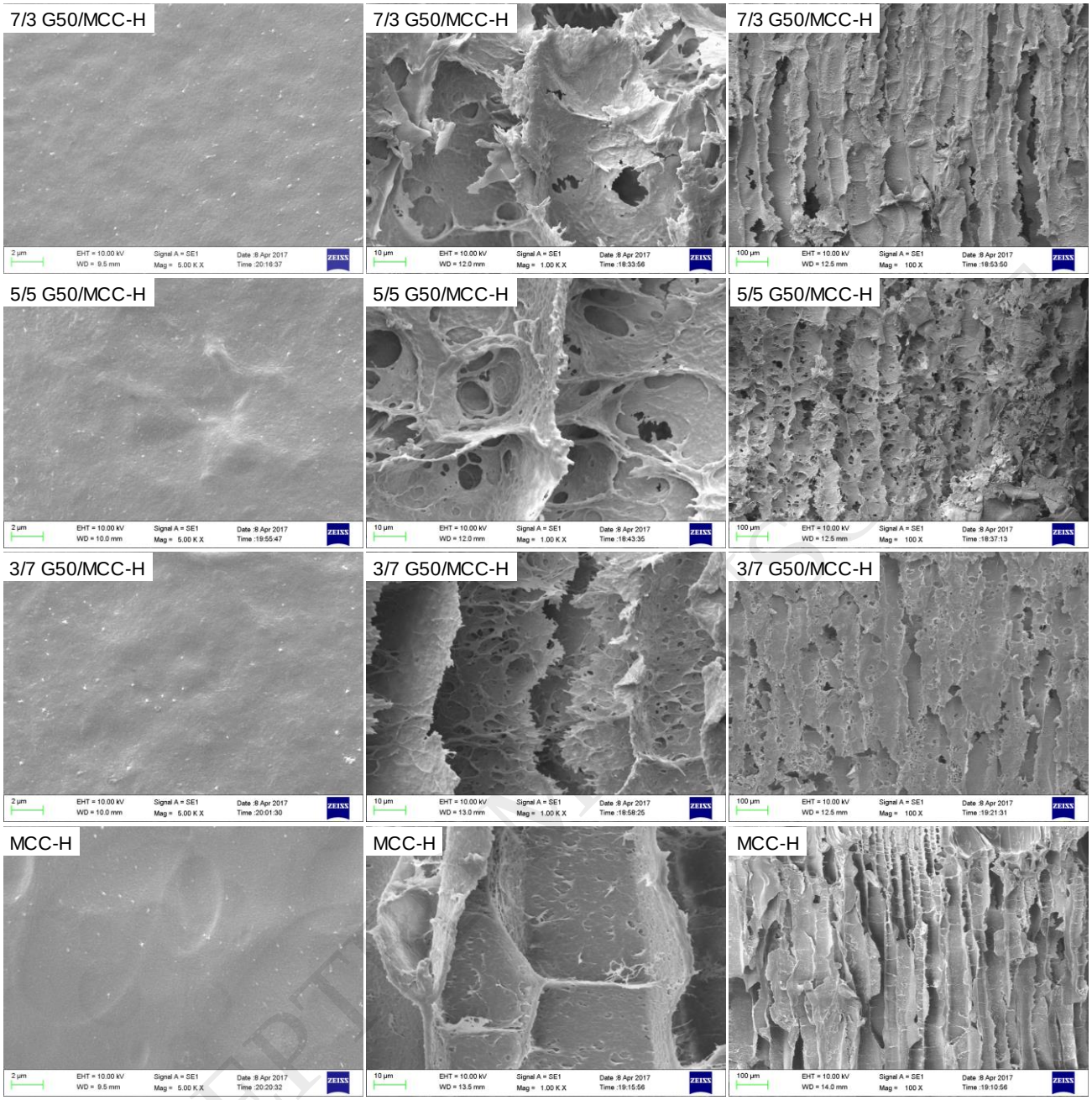

Fig. 1. SEM images of the surfaces and cross-sections of G50/MCC gels.

Fig. 1 also shows the SEM images of the cross-sections of G50/MCC gels with different ratios, where a porous structure can be seen. The ×100 magnification images (in the right column) show that MCC-H had a distinct longitudinal channel structure, whereas this feature was less apparent for the formulations containing starch (7/3 G50/MCC-H, 5/5 G50/MCC-H, and 3/7 G50/MCC-H).

Regarding this, it was possible that cellulose was more capable of providing a supporting effect on the structure. Moreover, as 3/7 G50/MCC-H seemed to have less solid and cohesive cell walls, we consider that the strong hydrogen-bonding interactions between starch and cellulose in the hybrid formulations (supported by the FTIR results in **Section 3.4**) might also limit such a structural supporting effect.

3.2 Nanoaggregation structure

The intensity distribution of SAXS is closely related to scattering distribution and electron density difference, so it can be used to analyze the nanoscale structure of materials, of which the perturbed or nonperiodic structures of amorphous and mesomorphic materials can be measured (Kuang et al., 2017; Wang et al., 2018). To better understood the nanoscale structure of G50/MCC gels, all the samples were tested in their hydrated state (gels). Fig. 2(a) shows the double-logarithmic SAXS patterns of G50/MCC gels with different G50/MCC ratios. No scattering peak could be seen, suggesting that these hybrid gels did not have a spatially periodic structure on the nanoscale. Lower *q* values led to higher scattering intensity. This could be due to the large difference between the network structure of the gels and the surrounding aqueous medium, resulting in increased scattering intensity, which mainly affected the intensity of scattered signals in small-angle regions (Tomšič, Prossnigg, & Glatter, 2008). With an increasing proportion of MCC, the network structure of G50/MCC gels became more compact, which affected the difference in electron density between the gels and the medium. The scattering strength of the gels followed the order: MCC-H > 3/7 G50/MCC-H > 5/5 G50/MCC-H > 7/3 G50/MCC-H.

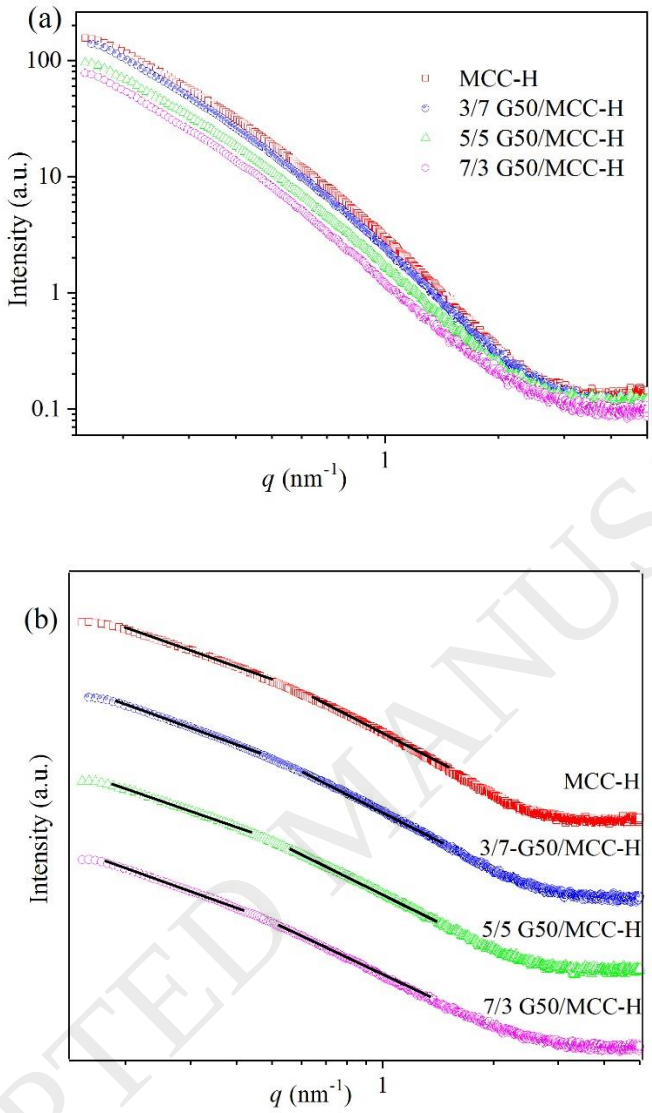

Fig. 2. Double-logarithmic SAXS patterns of G50/MCC gels with different ratios (a) and the $I \sim q^{-\alpha}$ relationships of SAXS patterns (b).

The fractal dimension indicated the compactness of a system (Beaucage, 1996) and has been used to describe the self-similar structure of gels (Tamon & Ishizaka, 1998). The material fractal structure could be obtained according to the changes in SAXS scattering intensity and be quantified

using fractal dimension *D*. In the low-*q* region, the curves comply with a simple power law equation, $I(q) \sim q^{\alpha}$, where the exponent α gives insight into the surface/mass fractal structure (Zhu, Li, Chen, & Li, 2012). More specifically, the mass fractal dimension ($D_m = \alpha$, $0 < \alpha < 3$) is used to indicate the compactness, whereas the surface fractal dimension ($D_s = 6-\alpha$, $3 < \alpha < 4$) is regarded as an indicator of the degree of smoothness of scattering objects. Additionally, the scattering objects of surface fractals are more compact than those of mass fractals.

In Fig. 2(b) and Table S1 (Supporting Information), the slop of the linear relationship could be represented by α, and all the hybrid gels had fractal structures in two linear regions. MCC-H had a mass fractal dimension ($D_{m1} = 1.98$) in the region of 14.41 nm < d ($d = 2\pi/q$) < 31.70 nm and had a surface fractal dimension ($D_{s2} = 2.84$) in the smaller size range of 2.96 nm < d < 8.27 nm, which indicates that there were two kinds of fractal scattering objects. The small scattering objects were compact surface fractals, corresponding to a denser network structure near the surface of the gel materials. The mass fraction of the scattering objects was relatively less compact, corresponding to near the middle part of the gel materials, which was consistent with the morphological observation by SEM.

The sample of 3/7 G50/MCC-H displayed two mass fraction dimensions ($D_{m1} = 1.94$ and $D_{m2} = 2.98$) in the range of 17.61 nm < d < 35.22 nm and 3.22 nm < d < 9.06 nm, respectively. Compared with MCC-H, 3/7 G50/MCC-H showed lower compactness in the mass fractal dimension region due to its D_m value (1.94) was lower than that (1.98) of MCC-H. and its scale ranges (17.61 nm < d < 35.22 nm and 3.22 nm < d < 9.06 nm) were larger than that (14.41 nm < d < 31.70 nm and 2.96 nm < d < 8.27 nm) of MCC-H. In other words, 3/7 G50/MCC-H had a looser structure and reduced density

of scattering objects than that of MCC-H. Again, we propose the skeleton structure of hybrid gels was mainly constituted by cellulose chains, whereas starch chains were evenly interspersed throughout the whole structure. Moreover, for the different gels, the α_2 values follow the order MCC-H > 3/7 G50/MCC-H > 5/5 G50/MCC-H > 7/3 G50/MCC-H, indicating that the addition of starch reduced the compactness of scattering objects.

3.3 Crystalline structure

Fig. 3 shows the XRD patterns of G50/MCC gels with different ratios. G50-H exhibited a V-type polymorph (amylose single-helices) indicated by the diffraction peaks at 2θ of 7.4°, 13.0°, and 20.4°. MCC-H displayed characteristic diffraction peaks at 2θ of 12.1°, 20.1°, and 21.4°, which represent a typical Type-II crystalline structure (Lu et al., 2015). G50-H showed very weak diffraction peaks, which could be ascribed to its lower crystallinity than that of MCC-H (18.4% vs. 47.5%, see in Table 2). Moreover, both 3/7 G50/MCC-H and 7/3 G50/MCC-H exhibited diffraction peaks mainly characteristic of the cellulose Type-II crystal structure. Regarding this, cellulose linear chains may have a higher tendency to undertake order arrangements, whereas starch chain rearrangements might be hindered by cellulose. For all the formulations, no new characteristic peaks were found.

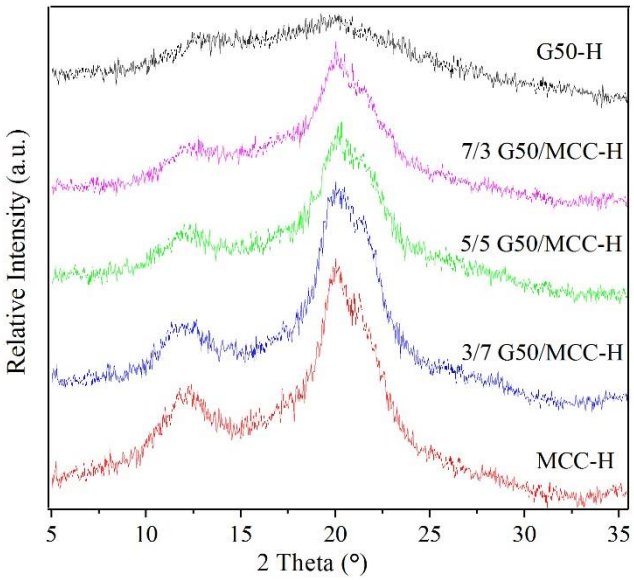

Fig. 3. XRD patterns of G50/MCC gels with different ratios.

3.4 Molecular interactions

ATR-FTIR was used to investigate the chemical interactions in G50/MCC gels and the results are shown in Fig. 4. Strong stretching vibration of ─OH groups could be seen in the region of 3600–3100 cm^{-1}, indicating the strong intra-/intermolecular hydrogen bonding in the hybrid materials (Moosavi-Nasab & Yousefi, 2011; Oh et al., 2005). The band in the region of 3000–2800 cm^{-1} should be attributed to the C─H stretching (Lan, Liu, & Sun, 2011). The characteristic FTIR absorption bands for G50-H and MCC-H were located at 2927 cm^{-1}, 2888 cm^{-1}, and those for 5/5 G50/MCC-H were at 2923 cm^{-1} and 2887 cm^{-1}. These bands could be associated with the C─H stretching of starch and cellulose. As shown in Fig. 4(c), the absorption peak for MCC-H at 897 cm^{-1} was caused by the deformation vibration of glucoside C1─H (Lan et al., 2011), which was the characteristic of cellulose β-glucoside. However, G50-H had no absorption peak at 897 cm^{-1}, and the characteristic peak for 5/5 G50/MCC-H was shifted to 894 cm^{-1}. Regarding this shift in position,

there could be hydrogen-bonding interactions between starch and cellulose chains. The bands for 5/5 G50/MCC-H well correspond to the characteristic bands for starch and cellulose, with no new characteristic peaks emerging. This was in agreement with a previous study (Liu & Budtova, 2012) where a composite film was prepared by dissolving amylopectin and cellulose in ionic liquid.

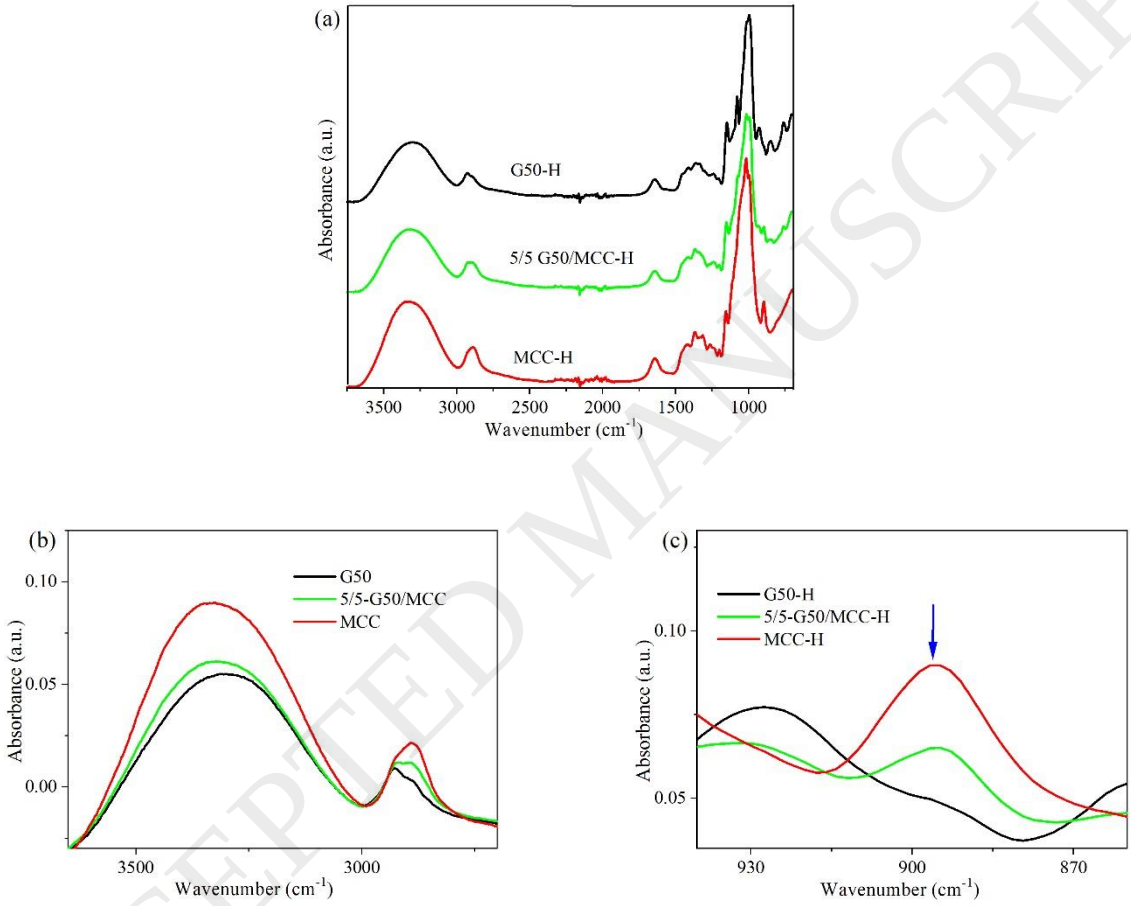

Fig. 4 Whole (a) and partial (b-c) ATR-FTIR spectra for G50-H, MCC-H and 5/5 G50/MCC-H.

3.5 Textural properties

Table 1 shows the TPA parameters of G50/MCC gels with different ratios. G50-H could not be formed and 7/3 G50/MCC-H could be destroyed during the test. Thus, the TPA data of these two

samples were not included here. It can be seen that with higher contents of MCC, the gels presented higher hardness values and thus higher deformation resistance. MCC-H had the strongest mechanical strength and highest resistance to deformation because of the strong intra-/intermolecular hydrogen bonding and the higher ordered structure in this material. For all the G50/MCC gels, the elastic values were around 0.88, indicating their excellent elasticity and recovery ability. Compared with 5/5 G50/MC-H, 3/7 G50/MCC-H and MCC-H had enhanced textural properties such as viscosity, cohesiveness, and recovery.

3.6 Equilibrium swelling ability

Table 2 summarizes the *ESR* of G50/MCC gels with different ratios. The data shows that the *ESR* of G50/MCC gels increased with an increasing proportion of G50. Regarding this, we propose the cellulose was less prone to absorb water due to its strong intra-/intermolecular hydrogen bonding and the dense structure, whereas the more flexible chains of starch could be beneficial to the swelling of the gels by water. However, 7/3 G50/MCC-H showed reduced *ESR* than that of 5/5 G50/MCC-H. In this case, the weak network structure resulting from the starch could reduce the water holding capacity of the hybrid material. Therefore, the G50/MCC ratio controls the *ESR* of gels, which is expected to further influence the drug loading and releasing properties.

3.7 Floatability

Fig. 5 shows that all the hybrid materials could immediately float on the surface of the water at 37 °C. After vacuum-freeze-drying, the water was removed but the original three-dimensional network structure of G50/MCC gels could be retained, which contributed to their lower density than that of water. G50/MCC gels were swelling and floating on the surface of the water for up to 36 h, suggesting it had an excellent, sustained floating capacity. After 36 h, some G50/MCC gels sank into the water, due to the increased density after the absorption of water. Our results demonstrate that G50/MCC gels had a good floating performance after vacuum-freeze-drying, which were instrumental in constructing low-density G50/MCC hybrid materials.

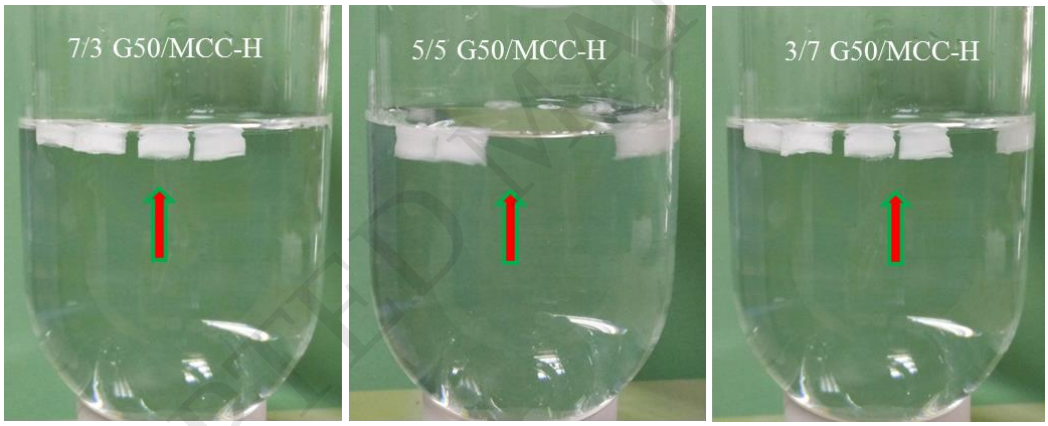

Fig. 5. Photographs taken during the buoyancy study of G50/MCC gels in water.

3.8 In vitro drug loading and releasing tests

Fig. 6 shows the pictures of G50/MCC gels and the resulting tablets after drug loading. It can be seen that the hybrid materials maintained a perfect tablet shape after drug loading and drying, which mean that they had good mechanical strength and structural stability. The drug loading contents for 7/3 G50/MCC-T, 5/5 G50/MCC-T, 3/7 G50/MCC-T, and MCC-T were 19.26%, 23.89%, 20.78%,

and 15.22%, respectively. With an increasing proportion of MCC, the ranitidine hydrochloride loading content was lower, which may be caused by a denser network structure contributed by cellulose. Nonetheless, the drug loading content for 7/3 G50/MCC-T was lower than that for 5/5 G50/MCC-T. Regarding this, with a starch content high enough, the network structure of 7/3 G50/MCC-T may become less stable, which was consistent with the results of equilibrium swelling ability.

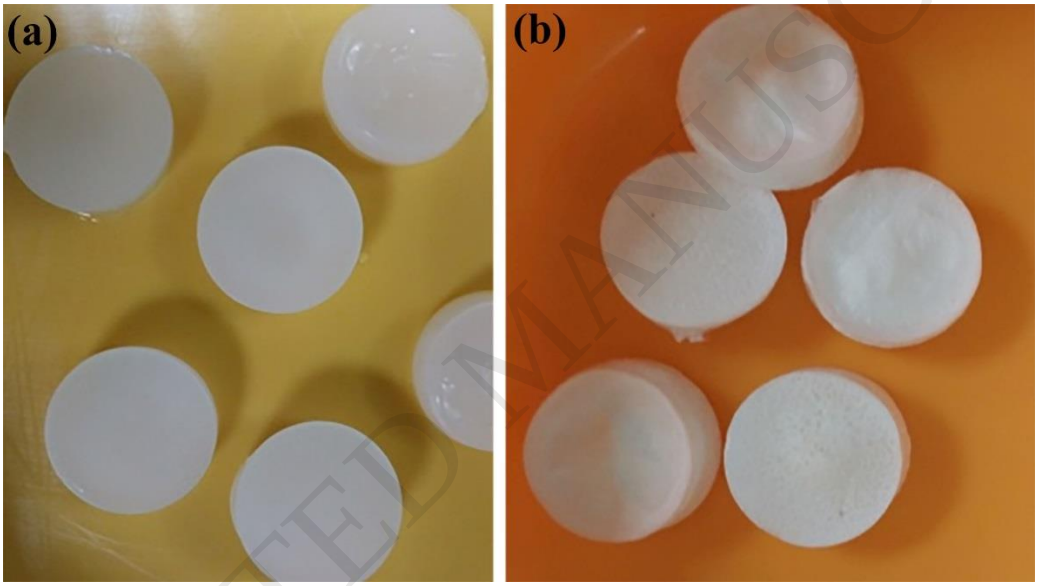

Fig. 6. Photographs of G50/MCC gels (a) and tablets after drug loading (b)

Fig. 7 shows the release curves for G50/MCC tablets as well as ranitidine hydrochloride capsules. The accumulated release percentages of ranitidine hydrochloride capsules were 62.16%, 97,27%, and 99.55% at 0.5 h, 1.5 h and 2 h, respectively. In comparison, G50/MCC tablets showed better-sustained release behaviors. The process of release could be divided into two stages: a rapid release phase between 0 h to 1 h and a slow release phase between 1 h and 10 h. As the proportion of

MCC was increased, G50/MCC tablets had a better-sustained release ability for ranitidine hydrochloride. The accumulate release percentages of 3/7 G50/MCC-T at 1 h, 4 h and 10 h were 45.87%, 75.08% and 100%, respectively. MCC-T had the lowest accumulated release percentage before 0.5 h, which could be due to its dense and stable surface structure. With increasing hydration, the accumulate release percentage after 1 h for MCC-T became higher than that of 3/7 G50/MCC-T. Despite the dense surface structure of MCC-T, its internal network structure contained hollow channels, which facilitated the release of ranitidine hydrochloride in a later stage. Besides, compared with that of MCC-T, the higher swellability of G50/MCC tablets may result in a better gel network structure after hydration, which should be instrumental in reducing the releasing rate as well.

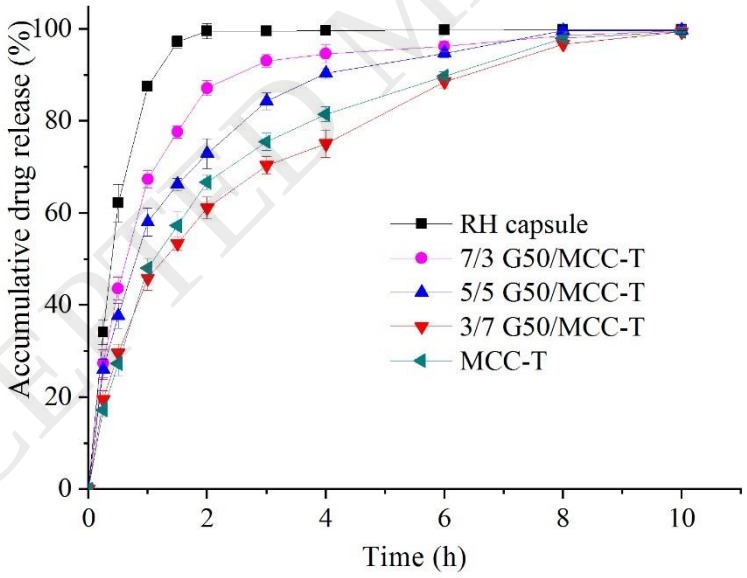

Fig. 7 The release curves of G50/MCC gels with different proportions and ranitidine hydrochloride (RH) capsules

Compared with ethyl cellulose ranitidine hydrochloride-loaded floating pellets (Saravanan & Anupama, 2011) and floating particles (Etman, Mahmoud, Galal, & Nada, 2016) as studied before, here we show the improved floating performance and sustained release properties presented by 3/7 G50/MCC-T. This formulation could release ranitidine hydrochloride faster within 1 h so that the drug could fully interact with H_2 receptors for effective treatment. A reduced releasing rate in a later stage could reduce side effects and enhance the efficacy of the drug. Thus, G50/MCC tablets developed in this work could be considered to be a good carrier of ranitidine hydrochloride and their excellent floating performance and sustained release behavior would be beneficial to improving the bioavailability of the drug.

Several regression equations of drug release kinetics of 3/7 G50/MCC-T were shown in Table S2 (Supporting Information). The *in vitro* simulated release data of 3/7 G50/MCC-T were checked for their compliance with zero-order, first-order, Higuchi, Hixon-Crowell, Ritger-Peppas, or Logistic models (Dave, Amin, & Patel, 2004). From the regression results of each kinetic model, the correlation coefficients (R^2) of first-order, Higuchi and Ritger-Peppas models were in the range of 0.9592–0.9853. The Ritger-Peppas model was found to be the most relevant, with its equation defined below (Sinclair & Peppas, 1984):

$$\ln Q = n \ln t + \ln k \qquad (4)$$

In this equation, Q is the solvent diffusion coefficient, k is the kinetics constant. If n is less than 0.45, Fickian diffusion predominates, whereas if n is greater than 0.89, the Case-II transport is the controlling transport mechanism (Ritger & Peppas, 1987). For G50/MCC tablets in the SGF, n is calculated to 0.37, less than 0.45, which indicates the Fickian diffusion release mechanism. In

addition, the Higuchi equation also reflects the diffusion mechanism. Therefore, we can conclude that ranitidine hydrochloride molecules were mainly released from the hybrid tablets by diffusion.

3.9 Mechanism of drug release

Fig. 8 shows our proposed mechanism of drug release. After G50/MCC gels were loaded with ranitidine hydrochloride, the drug molecules were dispersed throughout the material and vacuum-freeze-drying could allow low-density G50/MCC tablets to be obtained with a maintained network structure (Fig. 8a). The surface structure of G50/MCC tablets remained intact after a complete release in the SGF, suggesting that the drug was not released by the way of the disintegration of G50/MCC tablets. The rapid release of the drug from G50/MCC tablets might be due to the continuous infiltration of the SGF and the rapid dissolution of ranitidine hydrochloride, resulting in the different concentration between the inside and the outside of G50/MCC tablets leading to osmotic pressure. Also, the rapid release could be due to the weak diffusion resistance of G50/MCC tablets in the initial stage. Our data indicate that a dense network structure and surface film and a better equilibrium swelling ability were beneficial for a slow release of ranitidine hydrochloride. With increasing soaking time, the swelling of G50/MCC tablets increased but the original shape was maintained (Fig. 8b). Swollen G50/MCC tablets could reduce the free diffusion of ranitidine hydrochloride. A decrease in the osmotic pressure between the inside and the outside of G50/MCC tablets also contributed to a decreased drug releasing rate.

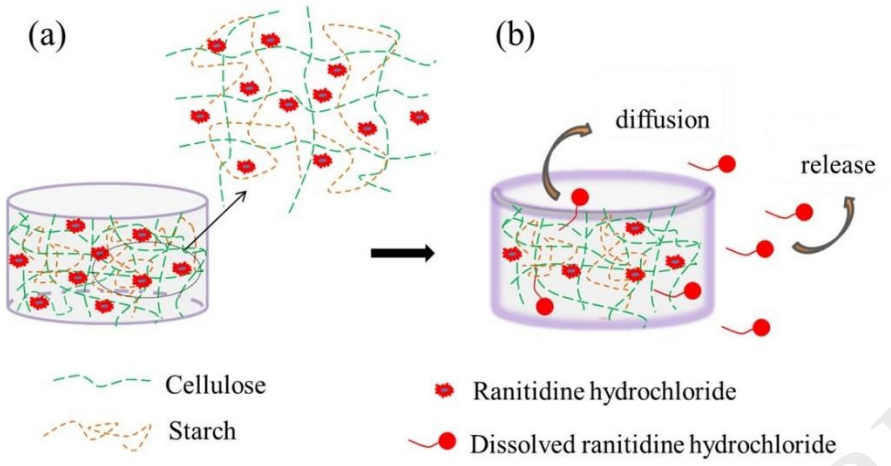

Fig. 8 The drug releasing mechanism of G50/MCC tablets

The ranitidine hydrochloride could be released through the interior network structure and the surface structure of G50/MCC tablets. Some properties of G50/MCC tablets affected their sustained release properties, such as the density and thickness of the surface film, internal network structure, and equilibrium swelling ability. In addition, the sustained release properties of G50/MCC tablets were also affected by the solubility of the model drug in the dissolution medium (SGF) and the diffusivity of the interior network structure and the surface structure.

4 Conclusion

In this work, we have developed G50/MCC gels that can be used as an excellent gastric-floating drug delivery system. The G50/MCC ratio has shown to strongly affect the structures (network structure, crystalline structure, and fractal structure) and properties (texture, *ESR*, and floatability) of the hybrid gels. A decrease in the G50/MCC ratio could lead to a more compact network structure of

the gels. Ranitidine hydrochloride was used as a model drug to be incorporated in the gels and low-density gastric floating tablets were produced by a vacuum-freeze-drying method. By modelling the release data, we propose that the drug release was both diffusion-controlled and osmotic pressure-driven. Our successful example here could provide technical and theoretical support for the rational design of gastric-floating drug delivery systems based on polysaccharide hybrid gels.

Acknowledgements

The authors from China would like to acknowledge the research funds from the National Natural Science Foundation of China (NSFC)–Guangdong Joint Foundation under a Key Project (No. U1501214), National Natural Science Foundation of China (NSFC) under a General Project (No. 31871751), and the Guangdong Provincial Government under a YangFan Innovative and Entrepreneurial Research Team Project (2014YT02S029). F. Xie acknowledges the support from the European Union's Horizon 2020 research and innovation programme under the Marie Skłodowska-Curie grant agreement No. 798225.

References

Arora, S., Ali, J., Ahuja, A., Khar, R. K., & Baboota, S. (2005). Floating drug delivery systems: A review. *AAPS PharmSciTech, 6*(3), E372-E390.

Beaucage, G. (1996). Small-Angle Scattering from Polymeric Mass Fractals of Arbitrary Mass-Fractal Dimension. *Journal of Applied Crystallography, 29*(2), 134-146.

Builders, P. F., Bonaventure, A. M., Tiwalade, A., Okpako, L. C., & Attama, A. A. (2010). Novel multifunctional pharmaceutical excipients derived from microcrystalline cellulose–starch microparticulate composites prepared by compatibilized reactive polymer blending. *International Journal of Pharmaceutics, 388*(1-2), 159-167.

Chen, J., Xie, F., Li, X., & Chen, L. (2018). Ionic liquids for the preparation of biopolymer materials for drug/gene delivery: a review. *Green Chemistry, 20*(18), 4169-4200.

Dave, B. S., Amin, A. F., & Patel, M. M. (2004). Gastroretentive drug delivery system of ranitidine hydrochloride: formulation and in vitro evaluation. *AAPS PharmSciTech, 5*(2), 77-82.

Etman, M. E., Mahmoud, E. H., Galal, S., & Nada, A. (2016). Floating ranitidine micro particulates: development and in vitro evaluation. *Int J Appl Pharm, 8*, 1-9.

Fassihi, R. (2004). Gastroretentive Delivery Systems: A Mini Review AU - Talukder, R. *Drug Development and Industrial Pharmacy, 30*(10), 1019-1028.

Forsyth, S. A., Pringle, J. M., & MacFarlane, D. R. (2004). Ionic liquids—an overview. *Australian Journal of Chemistry, 57*(2), 113-119.

Froschauer, C., Hummel, M., Iakovlev, M., Roselli, A., Schottenberger, H., & Sixta, H. (2013). Separation of hemicellulose and cellulose from wood pulp by means of ionic liquid/cosolvent systems. *Biomacromolecules, 14*(6), 1741-1750.

Gross, R. A., & Kalra, B. (2002). Biodegradable Polymers for the Environment. *Science, 297*(5582), 803-807.

Kadokawa, J.-i., Murakami, M.-a., Takegawa, A., & Kaneko, Y. (2009). Preparation of cellulose–starch composite gel and fibrous material from a mixture of the polysaccharides in ionic liquid. *Carbohydrate Polymers, 75*(1), 180-183.

Kansal, S., Garg, G., Awasthi, R., Singodia, D., & Kulkarni, G. T. (2011). Gastroretentive dosage forms: A review with special emphasis on floating drug delivery systems AU - Pawar, Vivek K. *Drug Delivery, 18*(2), 97-110.

Klemm, D., Heublein, B., Fink, H. P., & Bohn, A. (2005). Cellulose: fascinating biopolymer and sustainable raw material. *Angewandte Chemie International Edition, 44*(22), 3358-3393.

Koganti, N., Mitchell, J., MacNaughtan, W., Hill, S., & Foster, T. (2015). Effect of granule organisation on the behaviour of starches in the NMMO (N-methyl morpholine N-oxide) solvent system. *Carbohydrate Polymers, 116*, 103-110.

Kuang, Q., Xu, J., Liang, Y., Xie, F., Tian, F., Zhou, S., et al. (2017). Lamellar structure change of waxy corn starch during gelatinization by time-resolved synchrotron SAXS. *Food Hydrocolloids, 62*, 43-48.

Lan, W., Liu, C.-F., & Sun, R.-C. (2011). Fractionation of bagasse into cellulose, hemicelluloses, and lignin with ionic liquid treatment followed by alkaline extraction. *Journal of Agricultural and Food Chemistry, 59*(16), 8691-8701.

Li, D., Zhang, X., & Tian, Y. (2016). Ionic liquids as novel solvents for biosynthesis of octenyl succinic anhydride-modified waxy maize starch. *International Journal of Biological Macromolecules, 86*, 119-125.

Liu, K., Tan, X., Li, X., Chen, L., & Xie, F. (2018). Characterization of regenerated starch from 1-ethyl-3-methylimidazolium acetate ionic liquid with different anti-solvents. *Journal of Polymer Science Part B: Polymer Physics, 56*(18), 1231-1238.

Liu, W., & Budtova, T. (2012). Ionic liquid: A powerful solvent for homogeneous starch–cellulose mixing and making films with tuned morphology. *Polymer, 53*(25), 5779-5787.

Lu, Q., Lin, W., Tang, L., Wang, S., Chen, X., & Huang, B. (2015). A mechanochemical approach to manufacturing bamboo cellulose nanocrystals. *Journal of Materials Science, 50*(2), 611-619.

Mathew, A. P., Oksman, K., & Sain, M. (2005). Mechanical properties of biodegradable composites from poly lactic acid (PLA) and microcrystalline cellulose (MCC). *Journal of Applied Polymer Science, 97*(5), 2014-2025.

Moosavi-Nasab, M., & Yousefi, A. (2011). Biotechnological production of cellulose by Gluconacetobacter xylinus from agricultural waste. *Iranian journal of biotechnology, 9*(2), 94-101.

Moursy, N. M., Afifi, N. N., Ghorab, D. M., & El-Saharty, Y. (2003). Formulation and evaluation of sustained release floating capsules of nicardipine hydrochloride. *Die Pharmazie - An International Journal of Pharmaceutical Sciences, 58*(1), 38-43.

Oh, S. Y., Yoo, D. I., Shin, Y., Kim, H. C., Kim, H. Y., Chung, Y. S., et al. (2005). Crystalline structure analysis of cellulose treated with sodium hydroxide and carbon dioxide by means of X-ray diffraction and FTIR spectroscopy. *Carbohydrate Research, 340*(15), 2376-2391.

Pang, J., Wu, M., Zhang, Q., Tan, X., Xu, F., Zhang, X., et al. (2015). Comparison of physical properties of regenerated cellulose films fabricated with different cellulose feedstocks in ionic liquid. *Carbohydrate Polymers, 121*, 71-78.

Ritger, P. L., & Peppas, N. A. (1987). A simple equation for description of solute release II. Fickian and anomalous release from swellable devices. *Journal of controlled release, 5*(1), 37-42.

Saravanan, M., & Anupama, B. (2011). Development and evaluation of ethylcellulose floating microspheres loaded with ranitidine hydrochloride by novel solvent evaporation-matrix erosion method. *Carbohydrate Polymers, 85*(3), 592-598.

Shang, X., Jiang, H., Wang, Q., Liu, P., & Xie, F. (2019). Cellulose-starch Hybrid Films Plasticized by Aqueous $ZnCl_2$ Solution. *International Journal of Molecular Sciences, 20*(3), 474.

Sinclair, G. W., & Peppas, N. A. (1984). Analysis of non-fickian transport in polymers using simplified exponential expressions. *Journal of Membrane Science, 17*(3), 329-331.

Stevenson, D. G., Biswas, A., Jane, J.-l., & Inglett, G. E. (2007). Changes in structure and properties of starch of four botanical sources dispersed in the ionic liquid, 1-butyl-3-methylimidazolium chloride. *Carbohydrate Polymers, 67*(1), 21-31.

Tamon, H., & Ishizaka, H. (1998). SAXS Study on Gelation Process in Preparation of Resorcinol–Formaldehyde Aerogel. *Journal of colloid and interface science, 206*(2), 577-582.

Tan, X., Li, X., Chen, L., & Xie, F. (2016). Solubility of starch and microcrystalline cellulose in 1-ethyl-3-methylimidazolium acetate ionic liquid and solution rheological properties. *Physical Chemistry Chemical Physics, 18*(39), 27584-27593.

Tan, X., Chen, L., Li, X., & Xie, F. (2019). Effect of anti-solvents on the characteristics of regenerated cellulose from 1-ethyl-3-methylimidazolium acetate ionic liquid. *International Journal of Biological Macromolecules, 124*, 314-320.

Tomšič, M., Prossnigg, F., & Glatter, O. (2008). A thermoreversible double gel: Characterization of a methylcellulose and κ-carrageenan mixed system in water by SAXS, DSC and rheology. *Journal of colloid and interface science, 322*(1), 41-50.

Vilarinho, F., Sanches Silva, A., Vaz, M. F., & Farinha, J. P. (2018). Nanocellulose in green food packaging. *Critical Reviews in Food Science and Nutrition, 58*(9), 1526-1537.

Wang, H., Liu, Y., Chen, L., Li, X., Wang, J., & Xie, F. (2018). Insights into the multi-scale structure and digestibility of heat-moisture treated rice starch. *Food Chemistry, 242*, 323-329.

Wang, S., & Copeland, L. (2013). Molecular disassembly of starch granules during gelatinization and its effect on starch digestibility: A review. *Food and Function, 4*(11), 1564-1580.

Wang, Y., Chang, C., & Zhang, L. (2010). Effects of freezing/thawing cycles and cellulose nanowhiskers on structure and properties of biocompatible starch/PVA sponges. *Macromolecular Materials and Engineering, 295*(2), 137-145.

Wendler, F., Persin, Z., Stana-Kleinschek, K., Reischl, M., Ribitsch, V., Bohn, A., et al. (2011). Morphology of polysaccharide blend fibers shaped from NaOH, N-methylmorpholine-N-oxide and 1-ethyl-3-methylimidazolium acetate. *Cellulose, 18*(5), 1165.

Wu, R.-L., Wang, X.-L., Li, F., Li, H.-Z., & Wang, Y.-Z. (2009). Green composite films prepared from cellulose, starch and lignin in room-temperature ionic liquid. *Bioresource Technology, 100*(9), 2569-2574.

Xia, G., Wan, J., Zhang, J., Zhang, X., Xu, L., Wu, J., et al. (2016). Cellulose-based films prepared directly from waste newspapers via an ionic liquid. *Carbohydrate Polymers, 151*, 223-229.

Yang, J., Xie, F., Wen, W., Chen, L., Shang, X., & Liu, P. (2016). Understanding the structural features of high-amylose maize starch through hydrothermal treatment. *International Journal of Biological Macromolecules, 84*, 268-274.

Zarski, A., Ptak, S., Siemion, P., & Kapusniak, J. (2016). Esterification of potato starch by a biocatalysed reaction in an ionic liquid. *Carbohydrate Polymers, 137*, 657-663.

Zhong, F., Yokoyama, W., Wang, Q., & Shoemaker, C. F. (2006). Rice starch, amylopectin, and amylose: molecular weight and solubility in dimethyl sulfoxide-based solvents. *Journal of Agricultural and Food Chemistry, 54*(6), 2320-2326.

Zhu, J., Li, L., Chen, L., & Li, X. (2012). Study on supramolecular structural changes of ultrasonic treated potato starch granules. *Food Hydrocolloids, 29*(1), 116-122.

Table 1. TPA parameters of G50/MCC gels with different ratios.

Sample	Hardness	Elasticity	Cohesiveness	Gumminess	Recovery
5/5 G50/MCC-H	76.11 ± 6.12^{b}	0.88 ± 0.05^{a}	0.61 ± 0.06^{a}	44.94 ± 5.31^{b}	0.26 ± 0.04^{a}
3/7 G50/MCC-H	195.40 ± 20.86^{b}	0.88 ± 0.06^{a}	0.74 ± 0.02^{a}	146.66 ± 15.84^{b}	0.36 ± 0.03^{a}
MCC-H	418.71 ± 48.64^{a}	0.89 ± 0.04^{a}	0.81 ± 0.04^{a}	313.21 ± 49.12^{a}	0.39 ± 0.04^{a}

The mean value ± standard deviation of duplicate analyses is given. Values with different letters within the same column differ significantly ($p < 0.05$).

Table 2. Equilibrium swelling ratios (*ESR*) and crystallinity (X_c) of G50/MCC gels with different ratios.

Sample	*ESR* (%)	X_c (%)
G50-H	–	18.4±0.1^{e}
7/3 G50/MCC-H	1088 ± 9^{b}	39.8±0.2^{d}
5/5 G50/MCC-H	1369 ± 17^{a}	44.7±0.8^{c}
3/7 G50/MCC-H	1013 ± 9^{c}	56.5±0.3^{a}
MCC-H	797 ± 11^{d}	47.5±0.2^{b}

The mean value ± standard deviation of duplicate analyses is given. Values with different letters within the same column differ significantly ($p < 0.05$).